Journal of Biomedical Optics 9(6), 1288–1296 (November/December 2004)

Retinal response of *Macaca mulatta* to picosecond laser pulses of varying energy and spot size

William P. Roach
Air Force Research Laboratory
Human Effectiveness Directorate
Optical Radiation Branch
Building 803
8262 Hawks Road
Brooks Air Force Base, Texas 78253-5214

Clarence P. Cain
Northrop Grumman Corporation
Information Technology Division
4241 Woodcock Drive, Suite B100
San Antonio, Texas 78228-1330

Drew G. Narayan
Duke University Medical Center
Department of Ophthalmology
Durham, North Carolina 27710

Gary D. Noojin
Northrop Grumman Corporation
Information Technology Division
4241 Woodcock Drive, Suite B100
San Antonio, Texas 78228-1330

Stephen A. Boppart
University of Illinois at Urbana-Champaign
Beckman Institute
405 North Mathews Avenue
Urbana, Illinois 61801-3028

Reginald Birngruber
Medizinisches Laserzentrum Lübeck
Peter-Monnik-Weq 4
Lübeck 23562 Germany

James G. Fujimoto
Massachusetts Institute of Technology
Electronic Engineering and Computer Science Department
Room 36-361
77 Massachusetts Avenue
Cambridge, Massachusetts 02139

Cynthia A. Toth
Duke University Medical Center
Department of Ophthalmology
127 Wadsworth Building Eye Center
Durham, North Carolina 27710

Abstract. We investigate the relationship between the laser beam at the retina (spot size) and the extent of retinal injury from single ultrashort laser pulses. From previous studies it is believed that the retinal effect of single 3-ps laser pulses should vary in extent and location, depending on the occurrence of laser-induced breakdown (LIB) at the site of laser delivery. Single 3-ps pulses of 580-nm laser energy are delivered over a range of spot sizes to the retina of *Macaca mulatta*. The retinal response is captured sequentially with optical coherence tomography (OCT). The *in vivo* OCT images and the extent of pathology on final microscopic sections of the laser site are compared. With delivery of a laser pulse with peak irradiance greater than that required for LIB, OCT and light micrographs demonstrate inner retinal injury with many intraretinal and/or vitreous hemorrhages. In contrast, broad outer retinal injury with minimal to no choriocapillaris effect is seen after delivery of laser pulses to a larger retinal area (60 to 300 μm diam) when peak irradiance is less than that required for LIB. The broader lesions extend into the inner retina when higher energy delivery produces intraretinal injury. Microscopic examination of stained fixed tissues provide better resolution of retinal morphology than OCT. OCT provides less resolution but could be guided over an *in vivo*, visible retinal lesion for repeated sampling over time during the evolution of the lesion formation. For 3-ps visible wavelength laser pulses, varying the spot size and laser energy directly affects the extent of retinal injury. This again is believed to be partly due to the onset of LIB, as seen in previous studies. Spot-size dependence should be considered when comparing studies of retinal effects or when pursuing a specific retinal effect from ultrashort laser pulses. [DOI: 10.1117/1.1805554]

Keywords: histopathology; laser; laser-tissue interaction; ophthalmology; optical coherence tomography; retina; ultrashort laser pulses; wound healing.

Paper 02058 received Aug. 23, 2002; revised manuscript received Mar. 17, 2004; accepted for publication Jan. 16, 2004.

1 Introduction

Retinal effects of picosecond laser pulses may vary significantly depending on the energy per pulse and laser spot size at the retina. Spot-size effects on threshold for retinal injury have been well documented (Cain et al.[1]). However, in contrast to continuous wave laser exposures, short duration laser pulses delivered at a small focus increase the likelihood for peak irradiances to surpass the threshold required to induce a plasma event within the eye. Thresholds for laser-induced breakdown (LIB) from ultrashort pulses of visible laser energy delivered to the retina without the aid of external focusing optics have been demonstrated experimentally by Cain et al.[2] using a model human eye. Figure 1 demonstrates the threshold irradiance for avalanche and multiphoton mediated LIB for ultrashort laser pulses using the Cain et al.[2] eye model and the laser system employed in this study. In that work, Cain and his coworkers discussed the fabrication of an artificial eye that mimicked the focusing geometry of the human eye. This artificial eye was used to measure several nonlinear optical phenomena believed to have impact on retinal damage

Address all correspondence to William P. Roach, U.S. Air Force Research Lab, Bldg 803/HEDO, 2650 Louis Bauer Dr, San Antonio, TX 78235-5215. Tel: 210-240-4817; Fax: 210-536-3903; E-mail: william.roach@brooks.af.mil

1083-3668/2004/$15.00 © 2004 SPIE

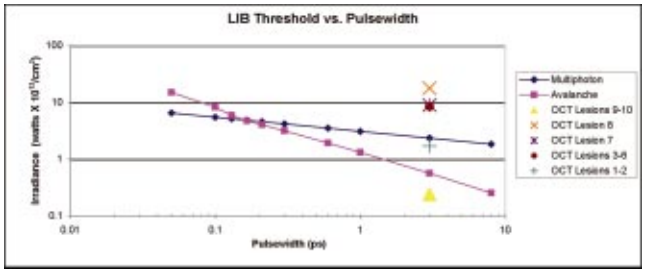

Fig. 1 Threshold irradiance for avalanche and multiphoton ionization, mediated LIB for ultrashort laser pulses (Cain et al.[2]). Note that OCT lesions 3 thru 8 (≤10-μm-diam laser spot size) have achieved irradiance levels that exceed the threshold for LIB in both processes. OCT lesions 1 and 2 have irradiance values sufficient to exceed the avalanche threshold. For OCT lesions 9 thru 17, the spot size is greater than or equal to 60 μm and the irradiance levels fall well below the threshold for either avalanche or multiphoton ionization.

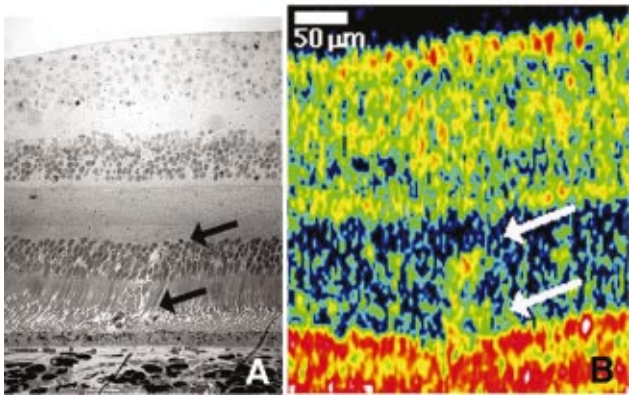

Fig. 2 (a) Light micrograph of 9-day-old lesion (3 ps, 4 μJ, and 10-μm spot-size). (b) OCT image of the same lesion. This very small (less than 20-μm horizontal lesion) site of disturbed photoreceptor nucleii with retinal pigment epithelium or macrophage migration into the photoreceptor outer segments was nonetheless visible on the comparable OCT scan. The arrows on the OCT point to the focal sites of increased reflectivity in the photoreceptor nuclear and inner segment zone of relative low reflectivity.

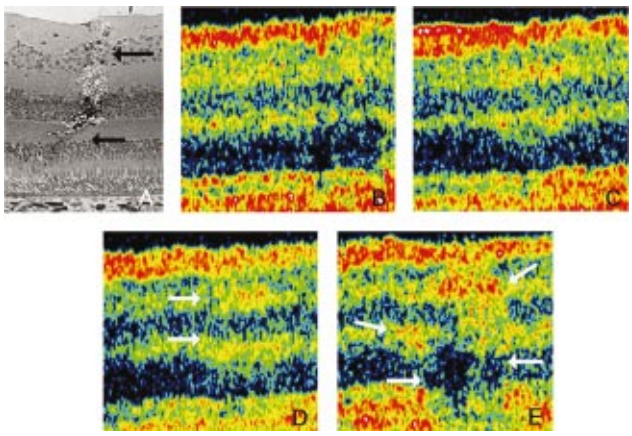

Fig. 3 (a) Light micrograph of 1-h, high-energy lesion (3 ps, 20 μJ, and 10-μm spot size). (b) OCT image of the site of the (a) lesion prior to laser delivery. (c) OCT image at 3-s postlaser delivery. (d) OCT image at 1 min postlaser delivery, and (e) OCT image at 1-h postlaser delivery. In (b) the baseline OCT demonstrates focal shadowing from a small blood vessel in the inner retina. The 3-s and 1-min scans both show a definite change in focal reflectivity of the inner and outer plexiform layers [arrows in (d)]. The lesion expands with focal low reflectivity in the photoreceptor layers. This could be due to shadowing from the inner retinal lesion. Note the larger zone of inner retinal damage without adjacent retinal pigment epithelium damage (also not seen in adjacent sections). Pyknotic nucleii are found in ganglion cell, inner nuclear, and photoreceptor nuclear layers, while there is swelling and vacuolization of adjacent tissue in a vertical band.

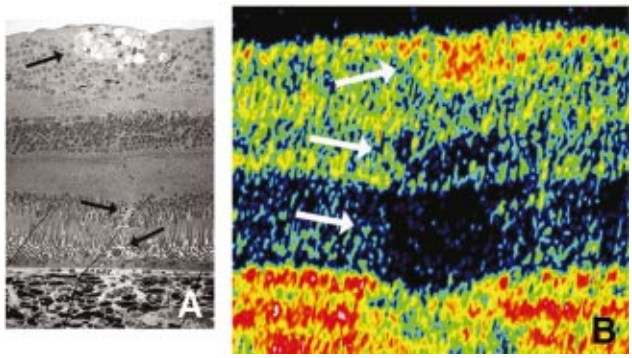

Fig. 4 (a) Light micrograph of a 9-day-old lesion (3 ps, 42 μJ, and 10-μm spot size) and (b) OCT image of the lesion at 9 days after laser delivery. Pigmented cells have migrated into the small focal site of photoreceptor damage, but anterior to this, there is a broad area of ganglion cell swelling with vacuoles and pyknotic nuclei. (b) Note that the OCT images the inner retinal damage as a more highly reflective site (top arrow) and shows shadowing of subsequent layers (lower arrows).

from ultrashort pulsed lasers, including LIB. Work by Toth et al.[3] demonstrated that LIB is a significant factor in suprathreshold fluence retinal laser lesions from 3 ps and 90 fs, where suprathreshold fluence is defined as fluence above thresholds that would produce a minimal visible lesion at the retina. From this work, low energy (<2-μJ) exposures demonstrated focal damage to the retinal pigment epithelial (RPE) with minimal photoreceptor or choriocapillaris effect. It is believed that these observations are due to melanosome-based focal-thermal and accompanying focal-acoustic damage to the RPE without spread to adjacent tissue.[2,4]

From these and other studies, it is proposed that greater energy delivered into a small focus will induce LIB events showing full-thickness retinal damage. If LIB is a mechanism of retinal damage from ultrashort pulses of visible laser light, then retinal response to picosecond pulses should vary not only with energy[3] but also with laser spot size across a range of energies. This study used optical coherence tomography (OCT) to detect and image retinal response by layer and over time, immediately after laser pulse delivery. Retinal response from the same exposure was measured at selected time intervals during the evolution of tissue reaction to exposure using both OCT and light microscopy observations of corresponding histology.

2 Materials and Methods

The treatment and procedures used in this study conformed to the use of animals in ophthalmic and vision research and Federal Guidelines. Animals used in this study were procured, maintained, and used in accordance with federal regulations, the Animal Welfare Act, the ''Guide for Care and Use of Animals'' NIH publication number 86-23m (prepared by the Institute of Laboratory Animal Resources, National Research Council), and the ARVO statement regarding the Use of Animals in Ophthalmic and Vision Research. The United States Air Force (USAF) Armstrong Laboratory at Brooks Air Force Base (AFB), Texas and Duke University, North Carolina, are both AAALAC accredited institutions.

Macaca mulatta of age approximately one to three years and weighing 3 to 4 kg were maintained under standard laboratory lighting conditions, were monitored and cared for during laser lesion placement, and were euthanized and enucleated as previously described.[5] Single laser pulses at visible wavelengths were delivered to the macular area, outside the fovea of each eye, as described previously by Cain et al.[5] Eight eyes of four animals were used for the *in vivo* and histologic study of 18 lesions. In the 1-h exposure, three lesions were produced in each eye and two lesions per eye in the remaining animals (see Table 1). Test sites received 3-ps, 580-nm laser energy. All laser energies reported for <20-μJ pulses are energies delivered to the cornea and either measured as a percentage of beam delivered to a beamsplitter, or determined from similar pulses delivered to a mirror and detector just prior to ocular delivery. Laser spot sizes were determined through diffraction-limited calculations and verified experimentally with the Cain et al.[6] eye model.

OCT images were obtained pre- and postlaser exposure using an experimental system, as reported previously.[7] To summarize the technical details of this system, the fiber-based OCT system utilized a Michelson-type interferometer and an 843-nm center wavelength superluminescent diode as a low-coherence light source. The coherence length in the eye was 10 μm (full width half maximum), which defines the longitudinal ranging resolution. The beam diameter at the cornea was 1.2 mm, which, neglecting ocular aberrations, results in an estimated 13-μm (full width half maximum) spot size on the retina. An optical power of 175 μW was incident on the eye and the signal-to-noise ratio of the OCT system (the maximum signal when the optical beam was reflected from a high-reflectance mirror, divided by the instrument noise level) was calculated to be 109 dB. A galvanometer-scanned retroreflector was used for reference arm pathlength delay and enabled 100 axial scans to be acquired in 2.5 s.

The OCT scanning and imaging optics were retrofitted onto a standard slit-lamp biomicroscope.[7,8] Two orthogonally mounted scanning mirrors provided lateral beam positioning on the retina. Retinal tomography was performed in a manner similar to indirect ophthalmoscopy using a $+60$-diopter double aspheric condensing lens mounted on the slit lamp in front of the eye to relay an image of the retina onto the slit-lamp image plane. An infrared-sensitive charge-coupled device (CCD) camera attached to the slit lamp enabled the position of the scanning OCT beam to be visualized in real time. For this study, the OCT imaging beam was aligned with the picosecond laser aiming beam. OCT beam scanning and data acquisition was user initiated and computer controlled. Cross sectional tomographic images [100 (horizontal)$\times$250 (vertical) pixels] of the retina were constructed by laterally scanning the light beam through the specimen and displaying longitudinal information from different adjacent transverse positions. The OCT-generated images represented the retinal structure based on the optical backscattered intensity, which was highly dependent on the optical properties of the structure. OCT images were taken in real time while viewing the fundus. Therefore, the position of the lesion on the OCT image is well correlated with what was seen on the fundus and later in histology.

The globes were incised anterior to the equator and immersed in a 3% gluteraldehyde and 0.1-M sodium cocodylate buffer immediately following enucleation. The posterior eyecup was cut away from the anterior segment after 10 min and replaced in the fixative. The macular area was later dissected and embedded in Spurr's resin and sectioned. The tissue sections were 1 μm in thickness and stained with methylene blue. Digital images were captured along with a 250-μm scale bar and scored for size of lesion and extent of damage into tissue layers. The size of the image was matched to the OCT using the micron scale bar in each image.

The retinal irradiance was calculated from the laser energy delivered divided by the area of the retinal laser spot size. This is reported for each lesion as retinal irradiance as terawatts per square centimeter (10^{12} W/cm^2 or tW/cm^2) in Table 1, column 4.

The extent of the lesion in sectioned retinal tissue was given a score based on the following criteria.

- A score of 0 indicates that there were no retinal, retinal pigment epithelial (RPE) or choriocapillaris abnormalities at the site of laser delivery, compared to adjacent normal retina.

Table 1 Summary of 3-ps laser lesions. In the 1-h exposure pathology, three lesions were produced in each eye and two lesions per eye in the remainder. Lesion 18 is a 5-ns lesion for comparison. Clinical appearance: RH is red hemorrhagic lesion in or beneath retina; VH is vitreous hemorrhage; WL is white retinal lesion. Pathology grade: H is hemorrhage.

Lesion number	Energy (μJ)	Beam diameter at retina (μm)	Retinal irradiance (TW/cm^2)	Clinical appearance of acute lesion	OCT-demonstrated location of lesion	Pathology grade of lesion	Age of lesion at OCT/pathology
1	4	10	1.70	WL	outer	2	9 days
2	4	10	1.70	WL	inner	4	9 days
3	20	10	8.50	WL	inner	4	1 h
4	20	10	8.50	WL	inner	4	1 h
5	20	10	8.50	VH	inner	5H	1 h
6	20	10	8.50	VH	inner	5H	1 day
7	21	10	8.91	VH	inner	5H	9 days
8	42	10	17.80	WL+RH	inner	3 to 4H	9 days
9	20	60	0.24	WL	outer	2	1 h
10	20	60	0.24	WL	outer	2	1 day
11	50	200	0.05	WL	outer	2	1 day
12	95	200	0.10	WL+RH	outer	3 to 4H	1 h
13	95	200	0.10	WL+RH	outer	3 to 4H	1 day
14	80	300	0.04	WL+RH	outer	3 to 4H	8 days
15	100	300	0.05	WL+RH	outer	3 to 4H	8 days
16	100	>300	>0.05	WL	outer	2	8 days
17	100	>300	>0.05	WL	outer	2	8 days
18	150	>300	>0.06	WL+RH	outer	3H+Bruch's membrane effects	1 h

- A score of 1 indicates that only RPE cells were affected at the laser site, usually appearing as a single disrupted or lifted cell.
- A score of 2 indicates that morphologic changes could be found in RPE cells, photoreceptor inner and outer segments, and photoreceptor nuclei, without inner retinal effects.
- A score of 3 indicates a lesion that extended through RPE cells and outer and inner retinal layers, but not into the nerve fiber layer.
- A score of 4 indicates a full-thickness retinal lesion involving RPE through nerve fiber layer.
- A score of 5 indicates a retinal lesion with rupture of the internal limiting membrane, which was usually associated with a vitreous hemorrhage.
- In addition, H indicates that a hemorrhage was visible in the tissue sections.

3 Results

Laser irradiances well above threshold for LIB for the 3-ps laser pulse almost always produced full-thickness retinal damage, in contrast to laser irradiances below threshold for LIB, which produced outer retinal damage sometimes associated with intraretinal hemorrhage. OCT imaging could be used to identify the location of laser effect within the retina. This was verified with the light microscopy of the retinal lesions.

We compare irradiance levels at the retina from this work to the threshold for LIB described elsewhere,[1,2] as shown in Fig. 1, where OCT lesions 1 and 2 had laser irradiances well above the calculated threshold for LIB via avalanche ionization, and OCT lesions 3 to 8 exceeded irradiance threshold levels for multiphoton ionization processes. For the OCT lesions 9 to 17, the irradiance levels achieved did not reach the critical fluence required for either ionization process, owing to an increasing laser retinal spot-size area as energy increased and exposure duration remained constant.

Imaging these lesions *in vivo* with OCT provided useful information regarding the location of injury within the retina. Inner retinal damage could be clearly differentiated from outer-retinal damage as seen in Fig. 2. The cluster of pixels of high reflectivity was present in each of the multiple scans of this lesion. The cluster of higher reflectivity corresponded to the site of the laser lesion, observed during scanning, and is

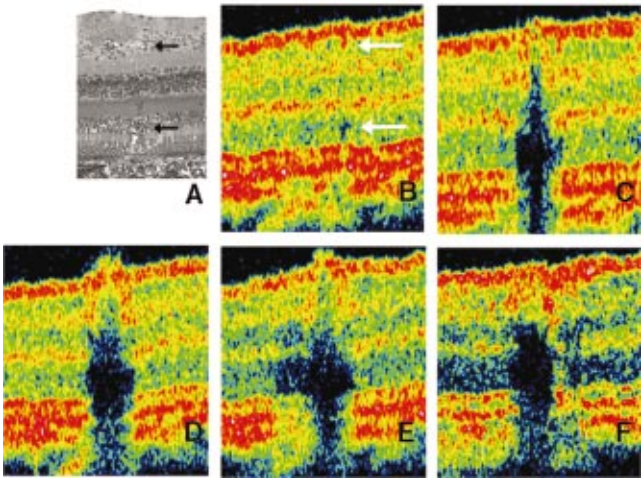

Fig. 5 (a) Light micrograph of 1-day-old lesion with vitreous hemorrhage (3 ps, 20 μJ, and 10-μm spot size). (b) OCT image of the site before laser delivery. (c) OCT image at 10-s postlaser delivery (3 ps, 20 μJ, and 10-μm spot size). (d) OCT image at 1-min postlaser delivery. (e) OCT image at 5-min postlaser delivery. (f) OCT image at 24-h postlaser delivery. The prelaser OCT scan included a retinal vessel with a focal shadow [arrows (b)]. After laser delivery, focal bleeding is seen into the vitreous cavity. This miniscule bleed could be observed by the researchers and on OCT produces a focal shadow in scans (c) through (f). The broadened area of low reflectivity of the outer retinal layers could be shadowing, or less likely other laser damage. Light micrographs demonstrate a very narrow column of full-thickness retinal damage along with extravasated blood in the inner retina.

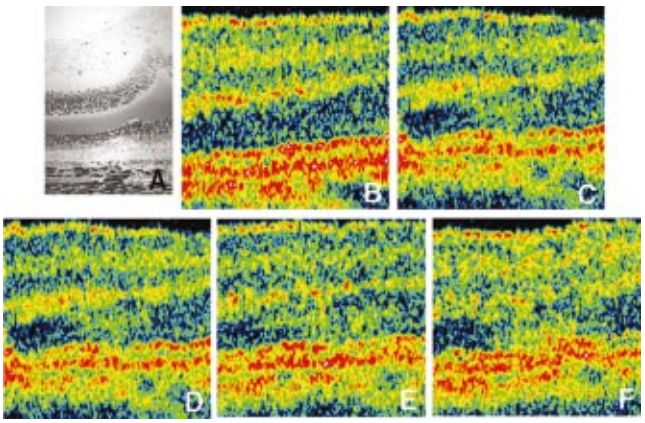

Fig. 7 (a) Light micrograph of 1-h lesion (3 ps, 20 μJ, and 10-μm spot size). (b) OCT image at prelaser delivery (3 ps, 20 μJ, and 60-μm spot size). (c) OCT image at 10-s postlaser delivery. (d) OCT image at 1-min postlaser delivery. (e) OCT image at 2-min postlaser delivery, and (f) OCT image at 38-min postlaser delivery. The light micrograph has a fixation artifact with some distortion. The retinal pigment epithelium is elevated from Bruch's membrane, and overlying photoreceptors are displaced. The inner retina appeared normal. The OCT images show a diffuse area of increased reflectivity in the photoreceptor layers (c) through (f) in contrast to (b) the prelaser scan.

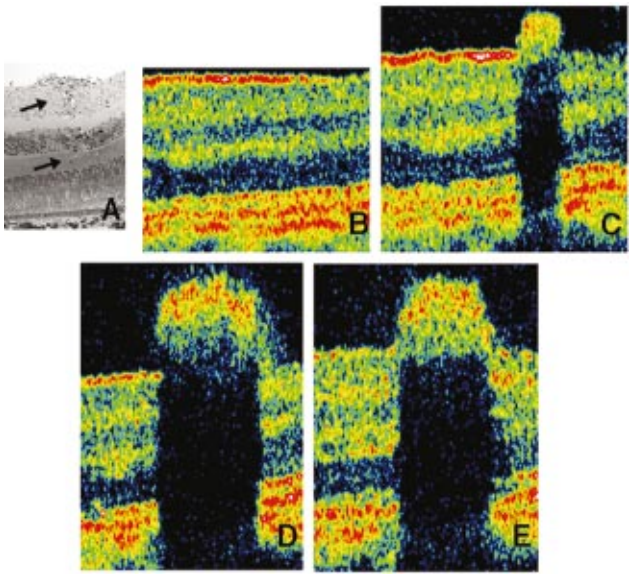

Fig. 6 (a) Light micrograph of 1-h lesion with vitreous hemorrhage (3 ps, 20 μJ, and 10-μm spot size). (b) OCT image at prelaser delivery. (c) OCT image at 4-s postlaser delivery with acute LIB hemorrhage producing a shadowing effect, which is a major drawback of OCT. (d) OCT image at 5-min postlaser delivery, and (e) OCT image at 32-min postlaser delivery. On the light micrograph, the blood could be seen extending from the vitreous cavity to the outer plexiform layer, but not deeper in the retina. The OCT images (c), (d), and (e) demonstrate the absence of data in the shadows of preretinal hemorrhage.

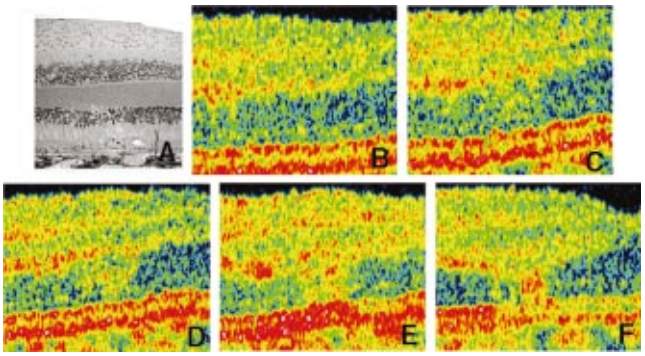

Fig. 8 (a) Light micrograph of 1-day-old lesion (3 ps, 20 μJ, and 60-μm spot size). (b) OCT image at prelaser delivery (3 ps, 50 μJ, and 200-μm spot size). (c) OCT image at 10-s postlaser delivery. (d) OCT image at 1-min postlaser delivery. (e) OCT image at 1-h postlaser delivery, and (f) OCT image at 24-h postlaser delivery. On the light micrograph the prominent outer retinal lesion is visible with retinal pigment epithelial migration and pyknotic photoreceptor nuclei. There is no disturbance anterior to the outer plexiform layer. On OCT images there are broad areas of higher reflectivity corresponding to the laser lesion. The reflectivity of the lesion appears to increase between 1 and 24 h after laser delivery. Note that pigmented cells have migrated into the lesion at 24 h and may be associated with this change.

different from the reflectivity pattern surrounding this site, as shown in the sample Fig. 2(b). The OCT changes that could be readily seen were a prominent focal increase or decrease in reflectivity relative to adjacent structures. Some lesions had a greater focal difference in relative reflectivity and thus were more prominent on OCT than other more diffuse lesions. For all the lesions, however, the focal changes in reflectivity were consistent in location in dozens of OCT scans over the laser delivery sites, and only selected captured images are shown in Figs. 2–8. For all lesions, the focal changes in retinal reflectivity on OCT became more prominent as the first 1 to 4 min passed after laser delivery. Similar patterns of focal high or low reflectivity were not seen in the nonlaser-treated retina, except for the typical shadowing patterns seen under major retinal vessels. None of these laser lesions were created near major retinal vessels. Retinal response differed by the peak irradiance delivered to the site. Seven of eight lesions 2 to 8 that received laser at irradiances well above LIB threshold demonstrated inner retinal damage on OCT and full-thickness injury in light micrographs, while one lesion that was imaged only at 9 days after laser delivery demonstrated outer retinal damage. All of the lesions created with irradiance below LIB threshold, lesions 9 to 17, demonstrated outer retinal effects, while lesions 12 to 15 also had associated inner retinal hemorrhage.

3.1 *Small Spot Size (10 μm) and Low Energy (4 μJ) Lesions (Lesions 1 and 2 in Table 1)*

The 10-μm spot-size laser area and 4-μJ lesions (1 and 2 in Table 1) were captured by OCT and light microscopy on day 9 postexposure. One lesion [Fig. 2(a) arrows], demonstrated a focal site of outer retinal vacuolization, debris, and RPE or pigmented macrophage migration into the photoreceptor layer. There was no focal visible change in choriocapillaris. The *in vivo* OCT demonstrated a corresponding focal site of relatively high outer retinal reflectivity [Fig. 2(b) arrows]. The other laser lesion, however, demonstrated inner retinal vacuoles and very minimal outer retinal damage in the light micrographs similar to, but smaller in lateral extent, to that seen in Fig. 4. There was a corresponding focal site of increased retinal reflectivity with outer retinal shadowing on OCT similar to, but over a narrower area than, Fig. 4. This was presumed, but not definitively due to the vacuoles, as a prelesion OCT was not performed.

3.2 *Small Spot Size (10 μm) and High Energy (20 to 42 μJ) Lesions (Lesions 3 through 8 in Table 1)*

The 1-h fixed tissue sections of the nonhemorrhagic lesions [Fig. 3(a)] demonstrated full-thickness retinal lesions with vacuolization adjacent to, but not directly over, the site of outer retinal injury. These lesions were prominent in the inner retina with pronounced vacuolization from the site of the ruptured internal limiting membrane to the inner nuclear layer in one lesion and into the outer plexiform layer in the other lesion. There were dense foci of pyknotic nuclei and underlying retinal pigment epithelial disturbance without vacuolization. The lesions examined at 8 or 9 days demonstrated inner retinal vacuolization out of proportion to the very focal photoreceptor damage. Retinal pigment epithelium appeared in double layers [Fig. 4(a)]. Choroidal layers appeared unaffected.

On OCT, the two nonhemorrhagic, high-energy, small spot-size lesions demonstrated a pattern of high relative reflectivity in the inner retinal layers with relative low reflectivity in outer retinal layers in the hour after laser delivery [Fig. 3(e)]. This began as very mildly increased reflectivity of the inner and outer plexiform layer by 3 s after laser delivery [Fig. 3(c)] in contrast to the prelaser appearance of the retina on OCT [Fig. 3(b)]. By 1 min, these sites in both lesions demonstrated pronounced increased reflectivity, along with a decrease in the typically intense nerve fiber layer relative reflectivity and decrease in relative reflectivity of the photoreceptors, retinal pigment epithelium, and choroid [Fig. 3(d)]. At 35 to 45 min, a decrease in reflectivity of the nerve fiber layer persisted and prominent increased reflectivity extended from the inner nuclear layer through the outer plexiform layer and possibly into the photoreceptor nuclei. Immediately adjacent to the inner area of high reflectivity, there was a pronounced low reflectivity with poorly defined margins at the level of the photoreceptors and extending slightly into the outer plexiform layer and choroid [Fig. 3(e)]. In another lesion examined at 9 days, inner high reflectivity was present with shadowing or relative low reflectivity of outer retinal layers [Fig. 4(b)].

Light micrographs of the hemorrhagic lesions at 1 h or 1 day demonstrated either preretinal hemorrhage with very little blood within the retina, or contained hemorrhage within the inner retina. These lesions demonstrated a site of photoreceptor damage less than 5 μm across and a site of retinal pigment epithelial damage less than 50 μm in diameter [Figs. 5(a) and 6(a)] without adjacent choriocapillaris changes.

In lesions with hemorrhages, using OCT, the high reflectivity of the hemorrhage and subsequent shadowing of the outer retinal layers depended on the thickness and location of the blood [Figs. 5(b) through 5(f) and 6(b) through 6(e)], although vacuole formation could also cause shadowing, as seen in Fig. 4(b). The hemorrhage was prominent within 4 to 10 s of laser delivery and increased in extent over subsequent minutes [Figs. 5(b) through 5(f) and 6(b) through 6(e)]. A focal site of preretinal hemorrhage shadowed all underlying retinal layers. In the 24-h lesion, the hemorrhage had cleared from the overlying retina. The retinal lesion demonstrated prominent inner retinal high reflectivity and outer retinal shadowing, possibly from erythrocytes in the inner retina or from the inner retinal vacuoles of the full-thickness narrow columnar lesion [Fig. 5(f)].

3.3 *Medium Spot Size (60 μm) 20-μJ Lesions (Lesions 8 and 9 in Table 1)*

With the same energy (20 μJ) but with the spot size increased to 60 μm, such as in lesions 8 and 9, the retinal response both by OCT and subsequent light microscopy demonstrated a broadened area of outer retinal injury rather than a full-thickness retinal lesion. The light micrograph of one lesion at 1 h demonstrates the 70-μm zone of retinal pigment epithelial damage with elevation of the RPE cells from Bruch's mem-

brane. The overlying injury extended only into the outer plexiform layer, with normal inner retina [Fig. 7(a)] and normal choriocapillaris.

OCT of the two lesions as they evolved supported the pathologic findings of one lesion at 1 h. At 8 s through 2 min, the lesions demonstrated outer retinal diffuse high reflectivity, with almost no change in reflectivity in inner retinal layers. By 36 min, the photoreceptor high reflectivity persisted with overlying low reflectivity in the outer plexiform layer. Again no notable inner retinal effect was appreciated. At 24 h, there was a pronounced site of relative high reflectivity in the photoreceptor layers in the other lesion.

3.4 *Large Spot Size (200 to 300 μm) and High Energy (50 to 100 μJ) Lesions (Lesions 11 to 18 in Table 1)*

Lesions produced with high laser energy and spot sizes varying between 200 to 300 μm demonstrated a different retinal pattern of injury. With examination by a light microscope when there was no vitreous hemorrhage (such as lesion 11 in Table 1), these lesions demonstrated a much broader area of outer retinal injury primarily affecting the RPE and overlying photoreceptors [Fig. 8(a)]. When there was retinal hemorrhage, the broad area of retinal injury extended into the outer nuclear, outer plexiform, and inner nuclear layers. There was almost no laser effect visible in the inner plexiform, nerve fiber layers, or choroidal layers. There were no narrow columns of injury or any pronounced vacuoles seen acutely or at 1 day in these lesions. At 8 to 9 days, one lesion with previous retinal hemorrhage demonstrated a small area of inner retinal vacuolization. The remainder of the lesions demonstrated outer retinal focal lesions.

The OCT of these developing lesions demonstrated a much broader area of increased reflectivity in the outer retinal layers that also extended into the middle retinal layers [Figs. 8(b) through 8(f)]. Except for one lesion with intraretinal hemorrhage, there was no pronounced high reflectivity of the middle layers relative to the outer retina (as was seen in the small lesions). No lesion demonstrated definite inner retinal change in reflectivity. There were no vitreous hemorrhages seen with these lesions.

4 Discussion

Numerous researchers have calculated and tested *ex vivum* the different ocular effects of the application of picosecond laser pulses.[9–15] Some of the studies have described the onset of the *in vivo* appearance of retinal injury after subnanosecond laser pulses were delivered.[16–18] Some of these studies used lenses to create a larger or fixed-size retinal laser spot, and thus a visible lesion that could be readily found for pathology. This increase in the retinal spot size of the laser beam from the diffraction-limited spot size of the eye thus increased the energy required to achieve threshold for LIB. Thus, columnar damage from LIB was not recognized as an injury event at moderately low levels of laser energy delivery until the morphology of small spot size lesions was examined by Toth et al.[3]

The current study has demonstrated that the variation in retinal response to picosecond laser pulses appears to be dependent on the spot size achieved at the retina. We found an intense predominantly inner retinal injury or column of full-thickness retinal injury in response to laser exposure to a 10-μm-diam spot at the retina (lesions 3 and 4). We believe this lesion was the result of LIB within the retina similar to that described in Cain et al.[5] This was in contrast to a confined broader outer retinal injury from delivery of similar laser energy over a larger retinal area (lesions 9 and 10). Those lesions we believe originated primarily from melanosome absorption of the laser energy in the RPE. Therefore, for a given spot size, we see outer retinal damage with low energy, and full-thickness damage and hemorrhage with energy above the threshold for LIB.

Previous work[3] of lower energy (<1 to 11 μJ) 3-ps laser pulses demonstrated partial to full-thickness retinal injury from 1.2- to 11.2-μJ laser pulses. When comparing the morphology of lesions from these studies, the horizontal extent of RPE damage increased minimally from low to high energy pulses (1.2 to 20 μJ), while the inner retinal area of injury increased greatly when greater energy was delivered. In both studies, inner retinal hemorrhages occurred. With hemorrhages, the confinement of the blood within the retinal layers defined the extent of lateral damage from the lesion. Thus, vitreous hemorrhages produced by the 20-μJ, small-spot, laser exposure in this study produced limited horizontal extent of retinal injury (40 μm), compared to the broad (>150 μm) inner retinal hemorrhages when there was no breakthrough of hemorrhage into the vitreous cavity after lower energy laser delivery. With high-energy delivery to a site 200 μm or greater, a retinal hemorrhage often occurred. There were no choroidal or choriocapillarial sites of bleeding found after careful microscopic examination of all hemorrhagic lesions, and all hemorrhages involved the retina above the outer nuclear layer, supporting the theory that these hemorrhages originate from retinal and not choroidal vessels.

The experimental OCT system was useful in capturing sequential images of relative retinal reflectivity as the lesions developed. The *in vivo* OCT images were, however, quite different from the light micrographs. With OCT, the tissue was examined with energy delivered to the surface of the retina and using alignment of signal reflected back from the different layers of the tissue into the Michelson interferometer. Thus there were great differences in OCT imaging in contrast to the light microscopy.

First, the depth of penetration of the signal into the retina and choroid determined the extent of the OCT examination. Deep choroidal structures could not be seen on OCT examination, and highly reflective components prevented signal penetration into deeper tissue. This was most obvious with cyst or vacuole formation or with bleeding, e.g., shadowing was prominent in Figs. 5 and 6 with pre- and intraretinal hemorrhage. One could not define whether outer retinal low reflectivity was a pathologic change or due to shadowing.

Second and third, the resolution of this OCT system was much more limited than light microscopy, and the OCT imaging of a lesion depended on a change in reflectivity relative to that of surrounding tissue. Small cellular elements could not be differentiated with OCT, though retinal layers and location of the lesion within these layers could be identified *in vivo*. The initial laser-induced tissue effect (first and second OCT scans over a lesion, 3 to 8 s) in some lesions may have been associated with no change in reflectivity or a change

beneath the level captured by this OCT system. In such a case, no perturbation would be seen on OCT (e.g., the lack of prominent OCT visible lesion in the first few seconds after 3-ps laser delivery). The subsequent tissue response to the initial injury (swelling, vacuolization, and pyknosis) may amplify the original lesion and produce focal areas of disturbed tissue that are large enough to be captured on OCT imaging by this system (e.g., the evolution of OCT lesions over time seen in Figs. 3, 7, and 8).

Despite these limitations to OCT imaging, over the time course of lesion development, tissue response followed a predictable pattern of high reflectivity at the site of initial laser effect, with adjacent low reflectivity as the lesion evolved. The timeframe of the evolution of bleeding could be followed with the development of shadowing on OCT. We could differentiate lesions with inner retina versus outer retinal changes in reflectivity from the laser energy. When inner retinal injury produced highly reflective lesions on OCT, we could not clearly determine the extent of associated outer retinal damage.

5 Conclusions

Of fundamental importance to industry, medicine, and research is a well-characterized, functional understanding of the mechanisms for laser-ocular interactions and how this might impact the extent of tissue effect and visual function.[19] Given the appearance of dependence of retinal pathologic response on the spot size of high-energy ultrashort laser pulses, we conclude that a careful spot-size study should be undertaken to analytically show this dependence as a critical component of observed retinal damage. The hypothesis would be that if the retinal spot size were larger than the diffraction-limited spot size used in laser safety studies, then onset of LIB observed in previous studies and resulting acute retinal response to the laser pulse exposure would be different, as demonstrated in this work but requiring further study. Thus one must be cautious in comparing data between studies, which used different retinal spot sizes in the evaluation of short laser pulse effects on the retina. This challenge is increased by the difficulty in directly measuring the diffraction-limited laser spot size at the retina.

In this work we demonstrate contrasting benefits in the two methods of imaging ultrashort pulse laser retinal lesions. Noninvasive OCT provides less resolution and minimal information at the subcellular level. However, since it is guided over the visible lesion by video observation of the aiming beam, retinal lesion sites are not missed. Because it is nondamaging and performed *in vivo*, repeated rapid OCT sampling over time could be performed at each lesion site, and lesion examination could be conducted with scans directed across a lesion of interest at any axis. We found, as in earlier work,[7] that OCT response over time for laser retinal lesions appear to correlate closely with subsequent pathology found with light microscopy. In contrast, the OCT pattern of early response to laser delivery more clearly elucidates the evolution of the injured site and demonstrates the early pattern of high reflectivity within the zone of injury. On the other hand, microscopic examination of stained fixed sections of excised tissue clearly provides the greatest resolution of retinal structure. Unfortunately, this information can only be gathered for each lesion at one time due to tissue excision, and the high resolution is only in one plane of imaging due to the disassembly of the tissue with sectioning.

Traditionally, laser safety studies have used fundus examination, fluorescein angiograms, histopathology of fixed tissue, and visual function testing to identify laser effects on the retina. *In vivo* information from OCT is a useful adjunct in such studies providing information, which will be useful in the clinical care of retinal disease. OCT data regarding normal retinal tissue and evolving retinal lesions are of use to clinicians applying this technique for human study and patient care. First, these correlate location of retinal structures within the OCT image. Second, these associate tissue elements or pathologic process with a pattern of relative reflectivity, which can aid in diagnosis. Third, these demonstrate use of OCT in monitoring wound healing or evolution of retinal pathology over time.

Despite high-energy laser delivery to create lesions, the pathologic response to the picosecond laser pulses remained confined to the retina. Retinal vasculature rupture occurred frequently in this study, with vitreous hemorrhage more common with smaller beam diameter at the retina. This information may be of use in developing therapies using laser-induced vascular anastamoses. The picosecond laser pulses at optimal beam diameter and energy may produce selective retinal vascular rupture with contained intraretinal hemorrhage. This is in contrast to lasers of longer pulsewidths where delivery parameters can be selected for choroidal vascular disruption.

Acknowledgments

We would like to acknowledge several individuals whose work the authors believe merit more than a mention at the end of this work. We wish to heartily thank Ewa Worniallo for her meticulous support of the histopathology effort, Katrina P. Winter for her continued work and coordination on the manuscript, Cheryl D. DiCarlo for her meticulous and intensive animal model work along with critical preparation of tissue for histopathology transport, Michael R. Hee for the OCT software development and operation during the experiments, and David J. Stolarski for his continued support of the manuscript, laboratory preparation and setup, and data analysis. The research was supported by the Air Force Office of Scientific Research (grants F49620-95-1-0266 and 2312AA-92AL014) and the USAF Armstrong Laboratory (contract F33615-92-C-0017).

The views and conclusions contained in this document are those of the authors and should not be interpreted as necessarily representing the official policies or endorsements, either expressed or implied, of the Air Force Office of Scientific Research (AFOSR) or the U.S. Government.

References

1. C. P. Cain, C. A. Toth, G. D. Noojin, D. J. Stolarski, S. Cora, and B. A. Rockwell, ''Visible lesion threshold dependence on retinal spot size for femtosecond laser pulses,'' *J. Laser Appl.* **13**(3), 125–131 (2001).
2. C. P. Cain, C. D. DiCarlo, B. A. Rockwell, P. K. Kennedy, G. D. Noojin, D. J. Stolarski, D. X. Hammer, C. A. Toth, and W. P. Roach, ''Retinal damage and laser-induced breakdown produced by ultrashort-pulse lasers,'' *Graefe's Arch. Clin. Exp. Ophthalmol.* **234**, S28–37 (1996).
3. C. A. Toth, D. G. Narayan, C. P. Cain et al., ''Pathology of macular

lesions from subnanosecond pulses of visible laser energy,'' *Invest. Ophthalmol. Visual Sci.* **38**, 2204–2213 (1997).
4. M. W. Kelly and C. P. Lin, ''Microcavitation and cell injury in RPE cells following short-pulsed laser irradiation,'' *Proc. SPIE* **2975**, 174–178 (1997).
5. C. P. Cain, C. A. Toth, C. D. DiCarlo et al., ''Visible retinal lesions from ultrashort laser pulsed in the primate eye,'' *Invest. Ophthalmol. Visual Sci.* **36**, 879–888 (1995).
6. C. P. Cain, G. D. Noojin, D. X. Hammer, R. J. Thomas, and B. A. Rockwell, ''Artificial eye for *in-vitro* experiments of laser light interaction with aqueous media,'' *J. Biomed. Opt.* **2**(1), 88–94 (1997).
7. C. A. Toth, R. Birngruber, S. A. Boppart et al., ''Argon laser retinal lesions evaluated *in vivo* by optical coherence tomography,'' *Am. J. Ophthalmol.* **123**, 188–198 (1997).
8. M. R. Hee, J. A. Izatt, E. A. Swanson et al., ''Optical coherence tomography of the human retina,'' *Arch. Ophthalmol. (Chicago)* **113**, 325–332 (1995).
9. B. Zysset, J. G. Fujimoto, and T. F. Deutsch, ''Time-resolved measurements of picosecond optical breakdown,'' *Appl. Phys. B: Lasers Opt.* **48**, 139–149 (1989).
10. A. Vogel, M. R. Capon, M. N. Asiyo-Vogel, and R. Birngruber, ''Intraocular photodisruption with picosecond and nanosecond laser pulses: tissue effects in cornea, lens, and retina,'' *Invest. Ophthalmol. Visual Sci.* **35**, 3032–3044 (1994).
11. D. X. Hammer, R. J. Thomas, G. D. Noojin, B. A. Rockwell, P. K. Kennedy, and W. P. Roach, ''Experimental investigation of ultrashort pulse laser-induced breakdown thresholds in aqueous media,'' *IEEE J. Quantum Electron.* **QE-32**, 670–678 (1996).
12. P. K. Kennedy, ''A first-order model for computation of laser-induced breakdown thresholds in ocular and aqueous media: Part I—Theory,'' *IEEE J. Quantum Electron.* **QE-31**, 2241–2249 (1995).
13. P. K. Kennedy, S. A. Boppart, D. X. Hammer, B. A. Rockwell, G. D. Noojin, and W. P. Roach, ''A first-order model for computation of laser-induced breakdown thresholds in ocular and aqueous media: Part II—comparison to experiment,'' *IEEE J. Quantum Electron.* **QE-31**, 2250–2257 (1995).
14. B. S. Gerstman, C. R. Thompson, S. L. Jacques, and M. E. Rogers, ''Laser-induced bubble formation in the retina,'' *Lasers Surg. Med.* **18**, 10–21 (1996).
15. C. R. Thompson, B. S. Gerstman, S. L. Jacques, and M. E. Rogers, ''Melanin granule model for laser-induced thermal damage in the retina,'' *Bull. Math. Biol.* **58**(3), 513–553 (1996).
16. A. J. Goldman, W. T. Ham, and H. A. Mueller, ''Ocular damage thresholds and mechanisms for ultrashort pulses of both visible and infrared radiation in the rhesus monkey,'' *Exp. Eye Res.* **24**, 45–56 (1977).
17. J. Toboada and W. D. Gibbons, ''Retinal tissue damage induced by single ultrashort 1060-nm laser light pulses,'' *Appl. Opt.* **17**, 2871–2873 (1978).
18. R. Birngruber, C. A. Puliafito, A. Gawande, W. Z. Lin, R. T. Schoenlein, and J. G. Fujimoto, ''Femtosecond laser-tissue interactions: Retinal injury studies,'' *IEEE J. Quantum Electron.* **QE-23**, 1836–1845 (1987).
19. J. Marshall, ''Structural aspects of laser-induced damage and their functional implications,'' *Health Phys.* **56**, 617–624 (1989).